Limnol. Oceanogr., 44(4), 1999, 1072–1080

Vertical secondary flows in submersed plant-like arrays

Heidi M. Nepf
Department of Civil and Environmental Engineering, Parsons Lab, Massachusetts Institute of Technology, 48-425, Cambridge, Massachusetts 02139

Evamaria W. Koch
Horn Point Laboratory, University of Maryland, P.O. Box 775, Cambridge, Maryland 21613

Abstract

Obstructions that protruded from a laboratory test bed into the benthic boundary layer were exposed to gradients in longitudinal velocity ($\partial u/\partial z$) that produced vertical pressure gradients along the surface of the obstruction. These pressure gradients generated vertical secondary flows that may have ecological significance for benthic fauna and aquatic macrophytes. Laboratory experiments demonstrated that secondary flows of up to 15% of the local longitudinal velocity were produced behind individual obstructions within a submersed plant-like or animal tube array and for conditions like those found in aquatic canopies or colonies. Our observations support theoretical predictions based on a reduced form of the Navier-Stokes equations, confirming that the ascending flow is controlled by a local balance of vertical pressure gradient, proportional to $\partial u^2/\partial z$, and viscous stress. The secondary flows were shown to transport dye from the bottom to a height dictated by the in-canopy current speed and turbulence intensity. By extension, the ascending flows can potentially contribute to the advection of nutrients from sediments, where they have been regenerated by microbial processes, to areas higher in the canopy, where they can be used by epiphytes and macrophyte leaves. Pressure gradients generated near the stem base also produce pore-water exfiltration. The coupled pressure-driven exfiltration and vertical advection have the potential to control nutrient availability in the bed.

Vertical secondary flows can occur behind obstructions that protrude from the sediments into the benthic boundary layer (e.g., Vogel 1994). The secondary flows are directed up the downstream face of the obstruction and form through the interaction of the protruding structure with the vertical gradient of longitudinal velocity in the benthic boundary layer (BBL). Some benthic worm populations have been observed to take advantage of this ascending flow by capturing particles brought up from the sediment (Carey 1983; Johnson 1988; Johnson 1990). The secondary flow was also observed behind black-fly larvae, which use both the longitudinal flow (u) and vertical flow (w) to capture particles from different locations (Chance and Craig 1986). The ascending flow can be disrupted by high population density, which results in skimming flow (Johnson 1990), a regime in which most of the current is redirected (skims) over the top of the organisms and flow between the organisms (roughness elements) is greatly reduced.

The ascending secondary flow may also occur behind the shoots of aquatic plants, such as marsh canopies, rice and reed fields, seagrass meadows, or vegetated river channels. Although several studies have documented larger-scale hydrodynamics within these systems, specifically the attenuation of mean currents and wave energy (Knutson et al. 1982; Gambi et al. 1990; Fonseca and Cahalan 1992; Hosokawa and Horie 1992; Ackerman and Okubo 1993; Leonard and Luther 1995; Koch 1996), only a few have examined smaller-scale, three-dimensional hydrodynamics; those that have focused on pollination (Ackerman 1983, 1986, 1997). Small-scale hydrodynamics may have additional ecological implications. Indeed, our study shows that vertical secondary flows as high as 15% of the local longitudinal velocity can develop at the base of individual stems and may rapidly carry nutrients up from the sediments, where they have been regenerated by microbial processes, to areas higher in the canopy, where they can be used by epiphytes and macrophyte leaves. Dissolved inorganic carbon (DIC) may be similarly transported and supplied to photosynthetic tissues more rapidly than previously estimated.

The objective of this study was to examine the magnitude of the ascending secondary flow at different population densities and current velocities. Although several researchers have previously observed the ascending flow behind generic boundary-layer obstructions (Woo et al. 1989; Eckman and Nowell 1984) as well as behind specific benthic organisms (Carey 1983; Chance and Craig 1986; Johnson 1988), this study represents the first effort to combine detailed quantitative observations with a theoretical flow analysis that considers both isolated elements as well as arrays. The analysis produces a predictive scaling law for secondary flows within plant habitats and other benthic colonies.

Acknowledgments

The authors thank Mark Luther for recognizing our complementary interests and encouraging our collaboration; Markus Hüttel for sharing his excitement about pore-water advection in seagrass ecosystems; and Becky Zavistoski for making the velocity measurements. Heidi M. Nepf was supported by a NSF CAREER Award, EAR 9629259.

Theoretical background

Obstructions protruding from the bed into the BBL are exposed to longitudinal velocity gradients ($\partial u/\partial z$) that produce vertical pressure gradients. These pressure gradients generate vertical secondary flows on the upstream and down-

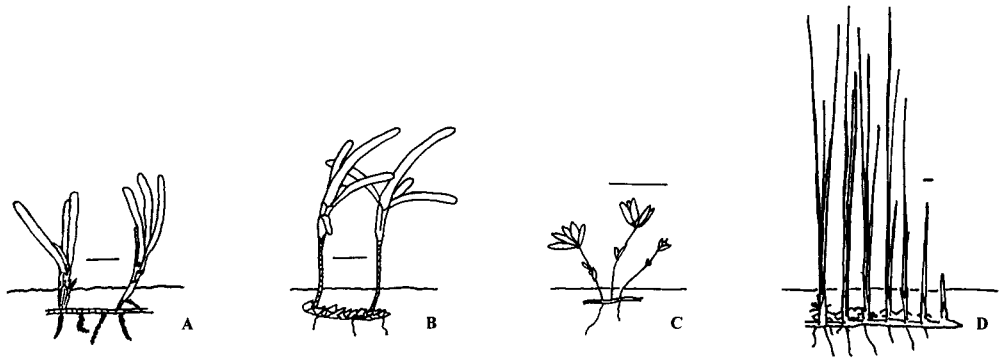

Fig. 1. Examples of seagrasses (a–c) and a marsh plant (d) that have cylindrical morphology near the bottom: (a) *Thalassia testudinum*, behind which the ascending flow was observed in the flume in Florida; (b) *Thalassodendron*; (c) *Halophila*; and (d) *Juncus*. The seagrasses are subtidal while the marsh plant is intertidal. Horizontal bar represents 3 cm.

stream faces of the obstruction. For simplicity, we considered a cylindrical obstruction representative of animal tubes (Eckman and Nowell 1984), reeds, and some species of marshgrasses and seagrasses, particularly near the stem base (Fig. 1).

The total surface pressure around the circumference of a cylinder is described by the pressure coefficient C_p (*see* Munson et al. 1990):

$$C_p = \frac{p - p_\infty}{\frac{1}{2}\rho u^2}, \tag{1}$$

where p is the local pressure at a point on the cylinder surface, p_∞ is the free stream pressure, ρ is the water density, and u is the velocity approaching the cylinder. The pressures p and p_∞ and the velocity u vary in z because of hydrodynamic forces and viscous stresses, respectively. It is important to note that the pressure coefficient, C_p, is not significantly affected by vertical shear, $\partial u/\partial z$, and remains nearly constant over the obstruction's span for both semi-infinite (Woo et al. 1989; Petryk 1969) and finite cylinders (Luo et al. 1996). Thus, variations in surface pressure can be inferred from Eq. 1, assuming C_p is constant in z, i.e.,

$$p(z) = p_\infty(z) + \frac{1}{2}C_p\rho u_\infty^2(z). \tag{2}$$

On the upstream face, stagnation occurs and $C_p = 1$. Since $\partial u/\partial z > 0$, i.e. u(z) increases with height away from the bottom, the stagnation pressure also increases away from the bottom. This positive pressure gradient creates a negative vertical velocity (w) on the upstream face. The fluid moving down the front face rolls up at the base of the cylinder, creating the familiar horseshoe vortex, which is subsequently swept downstream on either side of the cylinder (*see* Eckman and Nowell 1984, fig. 1).

According to potential flow theory, C_p should equal 1 on the downstream face as well. In real flows, however, viscous effects and flow separation decrease the downstream pressure and C_p becomes negative. The specific value of C_p on the downstream face depends on both the cylinder Reynolds number, $Re_d = ud\nu^{-1}$ (where d is the cylinder diameter and ν is the kinematic viscosity), as well as the turbulence intensity (Zukauskas 1987). For $Re_d \approx 10$–10^5, the pressure coefficient, $C_p \approx -0.6$ to -1 (Grove et al. 1964; Munson et al. 1990). The coefficient increases (moves toward zero) with increasing turbulence (Zukauskas 1987) and with $Re_d > 10^5$ (i.e., when the cylinder boundary layer becomes turbulent). With $C_p < 0$, the pressure gradient on the downstream face will be negative ($\partial p/\partial z < 0$), and it will drive an upward flow as shown in Fig. 2a.

Using Eq. 2 to represent the vertical pressure gradient, we can evaluate the vertical component of the momentum equations to determine the magnitude and vertical structure of the resulting secondary flow. Assuming steady conditions and a negligible contribution from the inertial terms, the momentum equation reduces to

$$0 = -\frac{1}{\rho}\frac{\partial P}{\partial z} - g + (\nu + \nu_t)\nabla^2 w \tag{3}$$

directly behind the obstruction, where g is the gravitational constant and ν and ν_t are the molecular and turbulent viscosities, respectively. Because $\nu_t \gg \nu$, except very close to the bed, we can drop the molecular viscosity term. It is interesting to note that previous analyses of cylinder secondary flows, which focused on individual cylinders at high Reynolds numbers, were inviscid (Starr 1966). Our investigation found that an inviscid theory was inadequate, and we attribute the difference both to lower Reynolds numbers (specifically, lower inertial effects) and to the augmentation of turbulent viscosity by the surrounding array. The force balance represented in Eq. 3 was verified by measurements reported in the Results section of this paper.

The stress term (last term in Eq. 3) depends on the spatial gradients of vertical velocity and thus on the dimensions of the secondary flow region. From flow visualization, the secondary flow scales on the cylinder diameter in width and length (∂y, ∂x) and on the boundary-layer height, δ, in the vertical coordinate (∂z), where δ is the height at which the shear ($\partial u/\partial z$) goes to zero. Because the flow region is more narrow than tall (∂x, $\partial y \ll \partial z$), the horizontal stresses dominate and the viscous term scales as $\nu_t w/(d/2)^2$, where the scale factor is absorbed into the parameterization of ν_t. Note

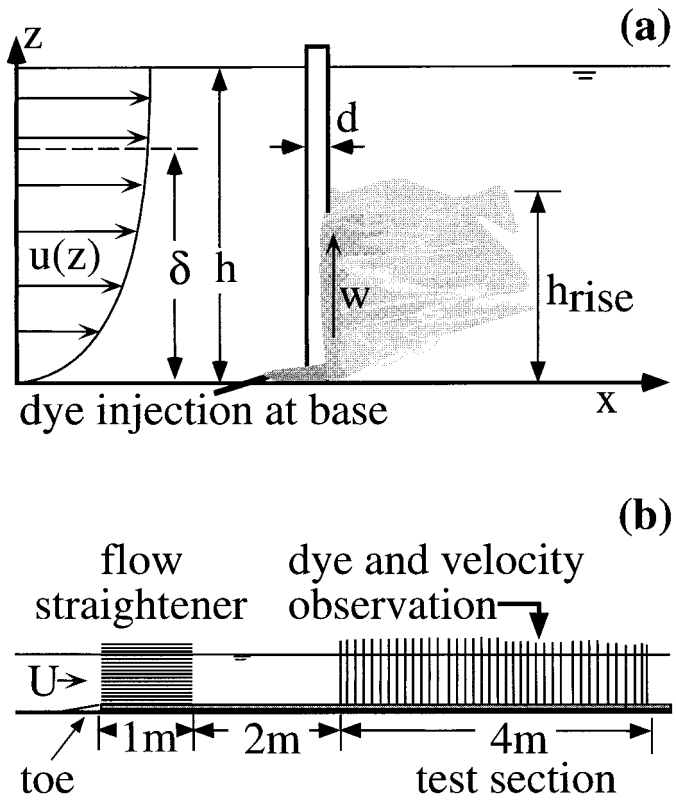

Fig. 2. (A) Schematic of dye visualization experiment that shows the vertical transport of dye (gray trace) by the vertical secondary flow generated on the back face of cylindrical obstructions protruding from the bottom into the benthic boundary layer. The rise height of the dye, h_{rise}, depends on the vertical advection, w, and the turbulent diffusion, D_t. (B)Schematic view of the 20-m recirculating flume. Plant-like arrays were constructed from 0.64-cm circular cylinders mounted onto Plexiglas boards. The cylinders extended through the entire water depth. The Plexiglas boards extended 3 m upstream of the array and ended in a toe that was tapered to the bottom to eliminate flow disruption.

that the gradients of velocity are defined by the half-width, i.e. d/2, because the velocity is greatest at the center of the flow region. Using Eq. 2 to define the pressure gradient, we arrive at

$$0 = -\frac{1}{\rho}\frac{\partial P_\infty}{\partial z} + \frac{1}{2}C_p\frac{\partial u^2}{\partial z} - g + \nu_t\frac{w}{(d/2)^2}. \quad (4)$$

Given that the free stream pressure is hydrostatic, $\partial P_\infty/\partial z = -\rho g$, the first and third terms cancel and the secondary flow is described by

$$w(z) = -C_p\frac{d^2}{8\nu_t}\frac{\partial u^2}{\partial z}. \quad (5)$$

Using $C_p = -1$, Eq. 5 indicates a positive vertical velocity on the downstream face, as we observed. Parameterization of eddy viscosity within an array was described in Nepf (1999). For $z > d$, the eddy scale is defined by the diameter of the obstruction, d, such that the eddy viscosity is given as $\nu_t = \kappa u_* d$, where $\kappa = 0.4$ is the von Karman constant, and u_* is the friction velocity of the bottom between obstructions. For $z < d$, $\nu_t = \kappa u_* z$.

A more general result can be found from Eq. 5 by assuming a logarithmic boundary layer profile within the canopy. This gives

$$w(z) = \frac{1}{8}u_* d\frac{\ln(z/z_o)}{\kappa^3 z}, \quad (6)$$

where z_o characterizes the roughness of the bottom between obstructions, i.e., excluding the form drag contributed by the obstructions.

The strength of the shear and the height of the BBL, δ, determine the magnitude and vertical extent of the secondary flow. If the obstruction height h_o is less than δ, then the region of vertical flow will be limited to h_o, as observed for live benthic feeders (Johnson 1988) and individual feeding-tube mimics (Eckman and Nowell 1984). However, the limited height of the obstruction does little to affect the above derivation, because C_p is unaffected by the finite cylinder height, except close to the free end (Luo et al. 1996). Specifically, C_p becomes less negative (decreases in magnitude) within two diameters of the free end, because the flow is increasingly three-dimensional (Luo et al. 1996). However, C_p remains negative to the tip, maintaining the upward secondary flow.

Without diffusion, the vertical extent of positive velocity dictates the height to which water parcels can be raised above the bottom (h_{rise}). However, h_{rise} can be limited by diffusion; i.e., solute or particles captured in the ascending flow may escape to the free stream through diffusive transport before traveling the full height of the flow region (Fig. 2a). The rise height is determined by comparing the time scale for horizontal diffusion to that of vertical advection. The diffusion time scale (t_D) is

$$t_D \sim \frac{d^2}{D_t}, \quad (7)$$

where the diameter, d, dictates the lateral dimension of the ascending flow region and D_t is the turbulent diffusivity. We focused on turbulent diffusivity because it dominates its molecular counterpart except very close to the bed. Assuming the turbulent Schmidt Number $Sc_t = \nu_t/D_t \approx 1$, then $D_t = \nu_t$. The time scale t_D represents the time required for dye to diffuse out of the ascending flow. With a vertical advection rate of w, the dye can be carried to a height given by

$$h_{rise} \sim wt_D \sim \frac{wd^2}{D_t}, \quad (8)$$

before it is completely released into the free stream and/or downstream wake. From Eq. 8 we see that h_{rise} decreases as D_t increases, i.e. as turbulence levels rise. The vertical advection, w, also decreases as turbulence levels rise and thus ν_t increases (see Eq. 5), so that increasing turbulence levels act through two mechanisms to decrease h_{rise}. Because turbulence levels have been shown to be a function of both free stream velocity and population density (Nowell and Church 1979; Eckman 1990; Nepf et al. 1997), we anticipate that h_{rise} will be a function of these parameters as well.

Methods

Experiments were conducted in a 20-m long by 38-cm wide recirculating, glass-wall flume at a flow depth of 15 cm (Fig. 2b). The depth (z) was defined as zero at the bottom and positive upwards, and the x-axis was positive downstream. The model array was constructed from wooden cylinders 6.4 mm in diameter. The cylinders were a reasonable surrogate in cross-section and rigidity for animal tubes (Eckman and Nowell 1984), reed stems, and the basal stem region of several seagrasses and marsh plants (Fig. 1). The cylinders were mounted onto 1.25 cm Plexiglas boards. The boards extended 3 m upstream of the array and were tapered to the bottom to eliminate flow disruption. Smooth inlet conditions were achieved by fibrous mats that damped inlet turbulence and a 1-m section of 0.6-cm honeycomb that eliminated swirl. The cylinders were arranged in a staggered array so that every fifth row was aligned longitudinally. The population density, n, was defined as the number of cylinders per base area. In addition to observing flows for a single, isolated cylinder, three values of n were considered: 210, 500, and 1,870 m^{-2}, corresponding to 0.6%, 1.4%, and 5.3% area coverage of the base.

The arrays differed from field conditions in that the population density was spatially uniform both horizontally and vertically (i.e., emergent). The uniform array was selected to uncouple velocity and population density so that each one's effect could be evaluated independently. Within a uniform array, the obstruction density directly controls the turbulence intensity (Nepf 1999). The unlimited cylinder length also allowed us to observe the maximum rise height for a given flow condition. As noted above, extrapolation to obstructions of finite height is straightforward, with the expected rise height equal to the lesser of the obstruction height, h_o, or the rise height determined for an unlimited obstruction. Extending results from uniform, emergent systems to nonuniform, submerged systems is discussed below.

Mean velocities, U, of 3–13 cm s^{-1} were considered. This range represents conditions within marsh/reed systems (Leonard and Luther 1995) and seagrass beds that colonize protected coastal areas (Worcester 1995; Grizzle et al. 1996; Koch 1996). The principal dynamics described in this study, however, would be unchanged when extrapolated to higher velocity ranges. Vertical profiles of the longitudinal (u) and vertical (w) velocities were measured using a two-dimensional laser Doppler velocimeter (LDV). Mean and turbulent velocity statistics were estimated from 100-s records sampled at 100 Hz. The measurement error for each record was ± 0.15 mm/s. To capture spatial variability within the array, multiple profiles were measured for each flow condition. The mean and turbulent velocities of each profile were then averaged to form a profile of bulk flow characteristics within the array (Nepf et al. 1997). Using the individual velocity profiles, the local shear velocity, u_{*i}, was estimated from the near-bottom values of Reynolds stress, i.e. $u_{*i} = \sqrt{\overline{u'w'}}$. The array bed-friction velocity, u_*, was taken as the average of the local values, u_{*i}. This estimator characterized the bottom drag only and excluded form drag associated with the obstructions. The bed-friction velocity, u_*, was used to assess eddy viscosity for Eqs. 5 and 6. Finally, profiles of vertical velocity, w, were measured 2 mm directly upstream and downstream of individual cylinders.

The flow field was also visualized using a neutrally buoyant blue dye (food coloring). The dye was injected at the bottom through a 20-cm-long syringe needle, following the technique described in Johnson (1988). As a second technique to aid visualization, crystals of potassium permanganate were distributed laterally in a line across the bottom, creating a continuous line source of dye. A back-lit white background produced excellent visual contrast, creating clear images of the dye movement. Half-centimeter markings on the test cylinder were used to quantify the vertical rise height of the dye. Finally, neither the dye visualization nor the laterally distributed velocity measurements suggested the presence of the flume-scale secondary flow commonly associated with noncircular channel cross-sections of small width-to-depth ratio (White 1986).

Similar dye visualization experiments were conducted within an array of natural seagrass (*Thalassia testudinum*, 384 shoots m^{-2}) in a 9×0.5 m laboratory flume at the University of South Florida. The submerged seagrass meadow was exposed to a mean current of 5 cm s^{-1} and a water depth of 16.3 cm. In addition, flow visualization was conducted within an emergent stand of *Spartina alterniflora* (Smooth Cordgrass) in the Great Sippewisset Marsh, Cape Cod, Massachusetts. The movement of dye injected at the bottom behind individual stems was recorded using an underwater camera.

Results

Velocity profiles—Profiles of the longitudinal velocity, u(z), are shown in Fig. 3 for each cylinder density: upstream of a single cylinder, i.e. free-stream (Fig. 3a); 210 cylinders m^{-2} (Fig. 3b); 500 cylinders m^{-2} (Fig. 3c); and 1,870 cylinders m^{-2} (Fig. 3d). The friction velocity for each case was 0.36, 0.40, 0.48, and 0.60 cm s^{-1}, respectively. The corresponding vertical velocity measured 2 mm downstream of an individual cylinder is given in Fig. 3e–h (closed circles). The general characteristics of the secondary flow agreed with our predictions. The maximum vertical velocity occurred near the bed, coincident with the maximum shear, $\partial u/\partial z$, and the vertical extent of the secondary flow roughly matched the boundary layer height, δ. As the array density increased, the near-bottom shear also increased, while shear over the rest of the profile (specifically $z > d$) was diminished because of greater vertical mixing. The vertical flow also decreased with increasing population density, indicating that it responded to the local (in z) shear, not the near-bed characterization, u_*. In other words, the vertical flow responded to the local balance of pressure and viscous stresses, and the vertical advection of momentum ($w\ \partial w/\partial z$) is unimportant, as assumed in Eq. 3. This finding can be further demonstrated by using the observed velocities to compare the magnitudes of the viscous terms and the dominant inertial term, $w\ \partial w/\partial z$, which scales as w^2/δ. The viscous term is O(10) times larger than the inertial term, indicating that the inertial terms can be neglected, as assumed in Eq. 3.

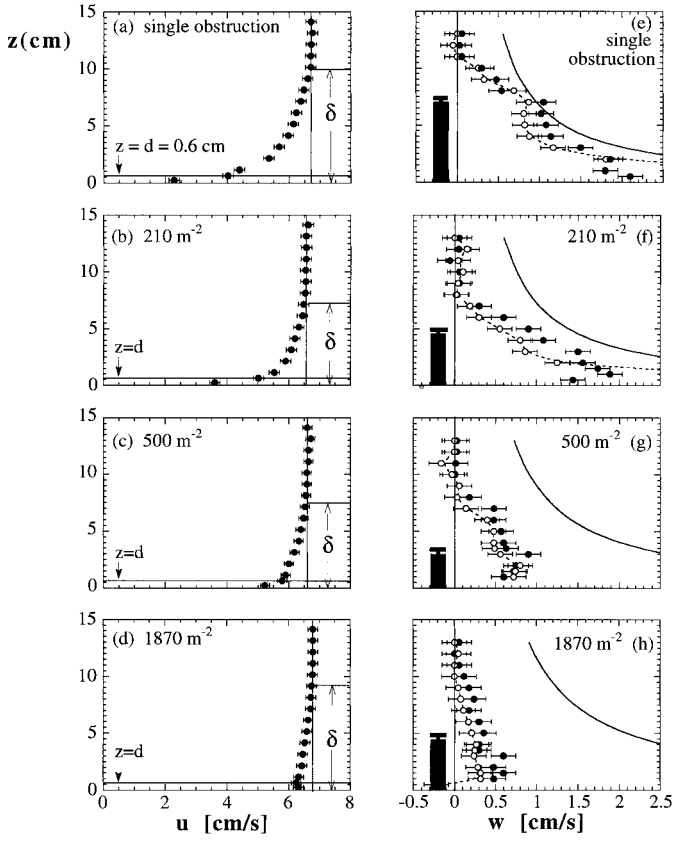

Fig. 3. Vertical profiles of longitudinal velocity (u) measured upstream of a single cylinder, i.e. free-stream velocity (a) and within arrays of population density n = 210 m^{-2} (b), 500 m^{-2} (c), and 1,870 m^{-2} (d). Profiles of vertical velocity (w) measured 2 mm downstream of a cylinder's downstream face are shown as dark circles for a single cylinder (e) and for a cylinder within an array of n = 210 m^{-2} (f), n = 500 m^{-2} (g), and n = 1,870 m^{-2} (h). The vertical velocity predicted from the measured longitudinal profile, u(z), and Eq. 5 is shown as open circles; it agrees well with the observed values. If a logarithmic form is assumed for u(z) (Eq. 6), the vertical velocity is overpredicted in most cases (solid line). The black column indicates observed rise height (h_{rise}) with standard error for dye injected at the bottom.

The decrease in ascending flow magnitude with increasing population density was also due to increasing turbulent viscosity, which diminished the vertical flow through turbulent exchanges of momentum to the outer flow. Although the turbulent viscosity was not measured directly, the magnitude of turbulent exchange was reflected in the levels of turbulence intensity. Turbulence intensity increased steadily with obstruction density, both within the ascending flow (0.08, 0.12, 0.18, 0.35) and within the bulk flow of the array (0.06, 0.16, 0.21, 0.39), where the values given are vertical averages for n = 1 cylinder, 210 m^{-2}, 500 m^{-2} and 1,870 m^{-2}, respectively.

For each case, the profile of longitudinal velocity, u(z), was used to evaluate the gradient, $\partial u^2/\partial z$, which was then used with Eq. 5 to predict the ascending flow, w(z) (open circles and dashed line in Fig. 3e–h). There was excellent agreement between the observed vertical velocities (closed circles, Fig. 3e–h) and those predicted by Eq. 5, again supporting the ideas that $w \sim u^2$ and that the local balance between viscous stress and pressure on which Eq. 5 was based accurately represented the physics of the system.

Within approximately one cylinder diameter of the bed, $z < d$, the predicted velocities deviated from the observed values. This was most apparent for the single obstruction and the 210 m^{-2} array, for which the predicted velocities (open circles and dashed line) extended beyond the axis limits for $z < d$. The observed vertical flow was diminished near the bed because the no-flux boundary condition forced $w = 0$ at $z = 0$. In natural systems this boundary condition may be relaxed ($w > 0$ at $z = 0$ is possible) if the porosity of the bottom is sufficient to permit exfiltration comparable to the vertical secondary flow. Larger near-bottom velocities would result (see discussion below on pore-water exfiltration).

Finally, the vertical velocity predicted with the assumption that u(z) is logarithmic, i.e. Eq. 6, is shown as a solid line in Fig. 3e–h. Because the laboratory flow was smooth turbulent with respect to the bottom boundary, $z_0 = \nu/9u_*$ in Eq. 6. For an isolated cylinder (Fig. 3e), the logarithmic prediction was reasonable, except near the bottom and approaching the top of the boundary layer, where u(z) naturally diverged from the logarithmic model. As the array density increased, the logarithmic model deviated from the measured profile u(z), specifically predicting more shear than observed; thus the logarithmic model progressively overpredicted the ascending flow. Clearly, the logarithmic law is not valid within an array.

This description of ascending flow reflects conditions for which velocity can be held constant as the population density increases. In the field, however, the in-meadow velocity is a function of stem or shoot density. The effect of stem density alone on the ascending secondary flow is more complex than observed in the controlled laboratory system.

Dye Rise Height—Black bars in Fig. 3e–h indicate the vertical rise height (h_{rise}) measured in the model array. In all cases, h_{rise} was smaller than the vertical extent of the ascending flow ($w > 0$), indicating that turbulent diffusion limited h_{rise}. Even though the turbulent viscosity and turbulent diffusivity were comparable, the velocity signature persisted over a greater vertical distance because the source of momentum, i.e. the pressure gradient, was distributed differently than the source of dye. As fluid rose from the bottom, mass exchange between the secondary flow and the free stream caused both dye and momentum to be lost to the free stream at comparable rates, i.e. $Sc_t = \nu_t/D_t \approx 1$. However, the dye concentration was attenuated more rapidly because it was only introduced at the bottom, whereas momentum was introduced over the entire boundary layer height by the pressure gradient throughout this region of shear.

Figure 4 demonstrates that the predicted values of h_{rise} (open circles) based on Eq. 8 matched the observed values (closed circles) within the model array, indicating that the correct scale dependence was captured by that calculation. The rise height decreased with increasing population density and with increasing longitudinal velocity, as both trends were accompanied by increasing turbulence and thus tur-

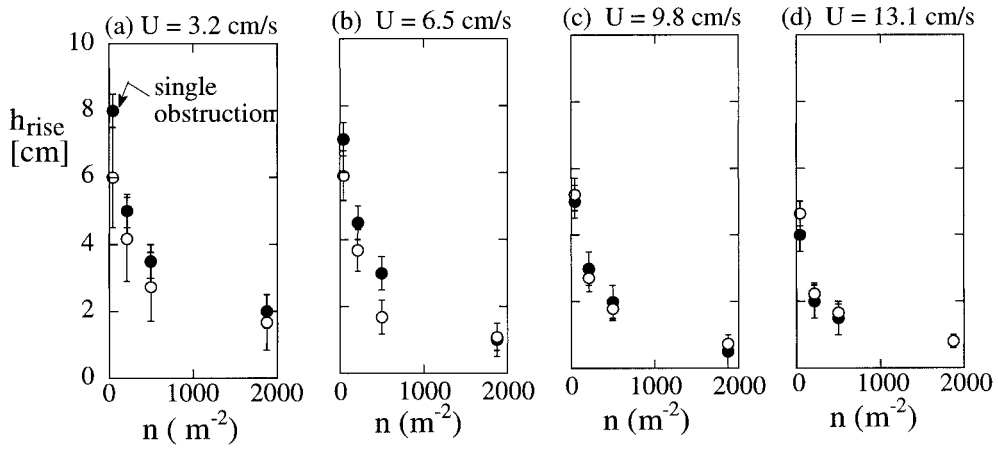

Fig. 4. Comparison of the observed (closed circles) and predicted (open circles) dye rise height, h_{rise}, within model cylinder arrays for four values of population density, n. In each graph the leftmost data pair corresponds to an individual cylinder. Bars indicate standard error. Each subplot represents a different mean velocity: U = (a) 3.2, (b) 6.5, (c) 9.8, and (d) 13.1 cm s^{-1}.

bulent diffusivity. The inverse relation between h_{rise} and U particularly reflected the dominant limiting function of turbulent diffusivity, because the rise height decreased, albeit weakly, despite an increase in vertical velocity associated with increasing longitudinal velocity. In addition, it suggests that the impact of the secondary flow may increase with slower flows.

The Peclet number, $Pe_w = (wh_{rise}) / D_t$, which compares the roles of vertical advection and diffusion, was evaluated using observed values of w and h_{rise} and assuming that vertical diffusivity was given by $D_t = \kappa u_* d$. Except for the densest array (n = 1,870 m^{-2}), $Pe_w > O(10)$, indicating that vertical transport near individual cylinders was dominated by advection within the secondary flow. However, for the highest population density Pe_w = (9, 4, 2, 2) for U = (3.2, 6.5, 9.8, 13.1 cm s^{-1}), respectively, suggesting that turbulent diffusion was becoming important to the local vertical transport.

Observations of vertical dye transport away from the bottom were also made in a test flume behind natural leaves of the seagrass *Thalassia testudinum.* These leaves are ribbonlike (20 cm long and 8 mm wide) with a relatively stiff base sheath and a flexible upper portion (Fig. 1). The flow around the base sheaths was similar to that within the model array, such that ascending flows were expected near the bottom of the canopy. Under a mean current of 5 cm s^{-1} the upper leaves bent in the direction of flow, redirecting some of the principal current over the top of the canopy. Thus, although no direct measurement of in-canopy flow was available, we expect that it was somewhat less than the mean current. As a reasonable approximation, we considered that the conditions at the base of the canopy were similar to those for the cylinder experiment under the lowest velocity, U = 3.2 cm s^{-1}. Observations and predictions for this velocity suggested a rise height between 3 and 5 cm for n = 384 m^{-2}, the canopy density (Fig. 4a). Indeed, the observed rise height within the seagrass canopy was h_{rise} = 3.5 cm, ending slightly below the bent area in the flexible leaf zone. Observations made in the field within a stand of *Spartina alterniflora* also confirmed the presence of near-bottom ascending flows behind individual stems. Dye rose 2–4 cm from the bottom, diverting from the stems just below the region of increasing stem/leaf density.

Discussion

Our laboratory experiments confirmed that ascending flows can be readily produced under flow conditions comparable to those found in aquatic systems and that the flow and associated vertical transport depend on both the current speed and the intensity of turbulence. The array conditions we studied were distinct from previous hydrodynamic studies of cylinder secondary flows, which focused on individual cylinders (Woo et al. 1989). Our results highlight how population density, by influencing both flow speed and turbulence, provide an important control on the strength of the secondary flow.

Extension to field conditions—The experiments were conducted in a uniform array so that velocity and population density could be manipulated independently, with population density largely controlling the turbulence intensity. In nonuniform systems such as plant canopies, this independence no longer holds and the in-canopy velocity decreases with increasing shoot density, which increases vegetative drag. The relationship between turbulence intensity and population density is more complex because it reflects the competing effects of reduced velocity and increased turbulence production by the obstruction wakes. These opposing tendencies produce a nonlinear response in which the turbulence levels initially increase but eventually decrease with increasing population density (Nepf 1999). This nonlinearity has been previously noted for emergent marsh vegetation (Burke and Stolzenbach 1983) and for flow within other bottom roughness elements (Eckman 1990). It may explain the apparent discrepancy between observations of turbulence levels within different seagrass canopies; that is, some studies report an increase (Gambi et al. 1990; Grizzle et al. 1996) and others

a decrease (Eckman et al. 1989; Ackerman and Okubo 1993) in turbulence within such communities. Although the specific relationships between population density, flow speed, and turbulence intensity are different in the real, nonuniform canopies, the scaling laws presented here are still valid. That is, given the in-canopy flow, u(z), and the turbulence intensity, which dictates D_t and ν_t, both the strength of the ascending flow, w, as well as the vertical transport scale, h_{rise}, can be predicted from Eqs. 5 and 8, respectively. The diminished mean flow observed within canopies would tend to reduce the ascending flow, while the diminished levels of turbulence intensity noted by some researchers (Ackerman and Okubo 1993; Worcester 1995) would promote it. However, the observations recorded in Fig. 4 suggest that turbulence intensity is more important than flow speed in controlling vertical transport. Specifically, h_{rise} decreased, albeit weakly, with increasing flow speed, indicating that the increasing diffusivity plays a larger role than the increasing dynamic forcing (u^2). Thus, quiescence within real canopies, in particular the low turbulence intensity and diminished turbulent diffusivity (Ackerman and Okubo 1993), should promote near-bottom vertical transport by this secondary flow mechanism.

Often real canopies also have vertical heterogeneity in plant biomass that affects the in-canopy current structure. For example, in some marshgrass (Leonard and Luther 1995) and seagrass (Koch 1996) species the near-bottom morphology, i.e., the sheath holding together the basal parts of the leaves or the short shoot supporting the leaves, produces less drag than the morphology higher up. In these cases, flow is intensified near the bottom, promoting the secondary flow in the basal region of the canopy. Moving up from the bottom, the velocity decreases as the vegetative drag increases, producing a near-bottom velocity maximum just below the transition to denser vegetation. Because an ascending flow will only be generated in regions of positive shear, $\partial u/\partial z > 0$, the vertical location of the near-bottom velocity maximum limits the vertical extent of the secondary flow. This control on the vertical rise height was suggested by the field observations in *Spartina alterniflora* described above: the ascending tracer diverged from the stems just below the point of increasing biomass density.

Finally, many aquatic plants are flexible and increase their angle of bending with increasing mean current speed (Fonseca et al. 1982). When the stem is inclined from the vertical, and in particular at inclinations greater than 30°, the plant shape is more streamlined and the pressure drop around the stem is reduced; i.e., the pressure coefficient, C_p, on the downstream face becomes less negative. This diminishes the pressure-induced secondary flow, as indicated by Eq. 5. When bent almost horizontal, the leaf can physically block a vertical flow. But even in systems with flexible leaf and upper stem regions, such as seagrasses, the near-bottom shoot is often stiff and cylindrical so that the conditions for an ascending flow are met at the base of the canopy. Consistent with this theory, we observed ascending flows of $h_{rise} = 3.5$ cm in the near-bottom region of the seagrass *Thalassia testudinum.* For this system, h_{rise} roughly corresponded to the bending point of the leaf, suggesting that the bending leaf did have some control over the maximum rise height. Finally, for dense meadows under conditions of extreme bending, the mean current is almost entirely deflected over the top of the canopy (skimming flow), so that flow within the canopy is greatly reduced or eliminated (Fonseca et al. 1982). This will reduce or eliminate the secondary flow as well.

Pressure-driven flows within the sediment—In addition to creating vertical transport within the water column, the pressure gradients produced by protruding stems may also generate flows within the sediment. Pressure-driven flows of this type have been observed near sand ripples (Huettel at el. 1996; Elliot and Brooks 1997*a,b*) and around organisms resting on or protruding from the bottom (Huettel and Gust 1992). As water flows over the bedform/object, regions of high and low pressure form at the front and the rear faces, respectively. This pressure gradient drives flow through the sediment. The exfiltrating current, which occurs at the rear face, may carry nutrients (N, Si, P) and DIC into the water column. If the obstruction is cylindrical, e.g. a grass shoot or feeding tube, the pressure gradient at the bed can be approximated from Eq. 2 and the obstruction diameter. Taking $C_p = 1$ and -1, at the front and rear face, respectively,

$$\frac{\partial P}{\partial s} = \frac{\rho U^2}{d}, \tag{9}$$

in which the pressure gradient is interpreted along the flow path through the sediment, s, which scales on the stem diameter, i.e. the distance between the extremes of pressure. Recall from above that on the rear face $C_p \approx -1$ even as $Re_D \rightarrow 1$, such that the pressure gradient given in Eq. 9 would be present even within the viscous sublayer. The exfiltration velocity, V_D, can then be estimated from Darcy's Law (Freeze and Cherry 1979):

$$V_D = K\frac{\partial P/\partial s}{\rho g} = \frac{KU^2}{gd}, \tag{10}$$

where K is the hydraulic conductivity, and g is the gravitational constant.

For typical values of K, the exfiltration velocity will be much less than that predicted for the secondary flow within the water column (*see* Eq. 5), so that the ascending flow will draw fluid from the water column as well as capturing the exfiltration. In addition, the mismatched boundary condition will constrain the secondary ascending flow near the bed ($z < d$), i.e. reduce it from Eq. 5, as discussed earlier. Finally, while the exfiltration current has been observed to transport particles of 1–10 μm, the current is too weak to dislodge particles at the sediment grain scale and thus does not appear to influence the depositional pattern around an obstruction (Huettel et al. 1996).

To confirm the validity of Eq. 10, we compared a predicted exfiltration rate with that observed for an array of polycheate tube mimics consisting of cylinders 0.6 cm in diameter protruding 1 cm above the bed (Huettel and Gust 1992). The following values are taken from Huettel and Gust (1992): $K = 1.5 \times 10^{-2}$ cm s^{-1} (= 15 Darcy), and $U = 8$ cm s^{-1} inferred for a logarithmic profile with $u_* = 0.5$ cm s^{-1} and the protruding height of the tubes. Using these values in Eq. 10, $V_D = 1.5 \times 10^{-3}$ cm s^{-1}. The exfiltration area A_e

$= 4\ d^2$ (fig. 1 in Huettel and Gust 1992) and the tube population density $n = 34\ m^{-1}$. The predicted rate of pore-water exfiltration was $[V_D n A_e] = 6.3$ liter $m^{-2}\ day^{-1}$, which compares well to the observed rate of 8.8 liter $m^{-2}\ day^{-1}$ (table 1 in Huettel and Gust 1992). Although limited to only one flow condition, the agreement between observed and predicted values suggests that Eq. 10 is accurate and can be used to assess the magnitude and thus the potential role of pressure-induced pore-water exfiltration, given the shoot diameter, the near-bottom, in-canopy current speed, and hydraulic conductivity of the sediment.

Implications of vertical flows within canopy, sediment, and water column—The combination of pressure-driven flows described above, i.e. pore-water exfiltration and ascending secondary flows, could create rapid movement of nutrients and DIC from interstitial waters to several centimeters into the water column. This direct advection between sediment and water column would circumvent the diffusive boundary-layer limitation on vertical exchange, supporting the recent review by Güss (1998) that questioned the molecular-diffusive-layer limitation for flows over porous surfaces. In addition, the vertical flows may control the availability and the vertical distribution of nutrient-enriched water, having important implications for biological function within an aquatic canopy.

The potential importance of this vertical transport mechanism depends on the in-canopy (colony) flow speed and turbulence intensity, which, as described above, are dictated by the mean current speed as well as the population density and flexibility of the vegetation (protruding structures). The pressure-induced pore-water advection increases with U (specifically, with U^2). But h_{rise} decreases with increasing U because of increasing diffusivity (Fig. 4 and Eq. 8). As a result, low near-bottom flow should create a small exfiltration flux but large vertical transport within the water column, while high near-bottom velocity should create a large exfiltration flux but limited vertical transport within the water column; that is, the exfiltrate would be trapped close to the bottom. The second regime is promoted by biomass distributions that decrease close to the bottom to produce near-bottom maximums in the velocity profile. This regime would produce maximum nutrient concentration near the bottom, which would benefit marshgrasses and seagrasses with basal meristems, i.e. whose young, actively growing tissue is located near the base of the plant.

As a second example of how vertical flows may affect canopy ecology, consider the observation that the growth rate of some freshwater and marine macrophytes is greatest at intermediate current velocities (Boeger 1992; Merrell 1996; Power 1996; Koch 1999). Because these plants can use nutrients from either the water column or the pore water, the following regimes of nutrient supply would apply: For low near-bottom flow, pore-water advection (Eq. 10) is small and nutrient regeneration from the bed is limited. The combination of low nutrient supply and relatively thick blade boundary layers, also the result of low flow speed, greatly reduces the flux between the leaf surface and the canopy water. In addition, the low pore-water exfiltration may allow phytotoxins like sulfide to accumulate in the sediment. For high in-canopy flow, pore-water advection is rapid, reducing nutrient availability to the roots. In addition, h_{rise} is small and the exfiltrated nutrients may not be carried high into the canopy to benefit the photosynthetic tissue and its epiphytes. Rapid exfiltration coupled with limited vertical transport could limit nutrients at both the root and the leaf levels, as suggested by Koch (1999). Consistent with this hypothesis, high flows do not negatively affect plant growth in cohesive sediments that have low hydraulic conductivity and thus exhibit limited pore-water exfiltration even under high flow conditions (Boeger 1992). Because both high and low flows limit growth, intermediate flow speeds are optimum. Pore-water advection would then be sufficient to reduce phytotoxins while enhancing the level of nutrients and DIC in the water column, and the secondary flow would be large enough to carry the nutrients and DIC vertically to the leaves while the sulfide was oxidized. Under these conditions plants could use nutrients from both the sediments and the water column.

In summary, we combined quantitative observation and theoretical flow analysis to describe the vertical secondary flow on the downstream face of cylindrical obstructions, both in isolation and within an array. The ascending flow reflected a local balance of vertical pressure gradient, proportional to $\partial u^2/\partial z$, and viscous stress. It was controlled by the in-canopy current speed and turbulence intensity, both of which depended on the population density. Scaling laws derived and confirmed in this study can be used to assess the importance of the secondary flow to near-bottom vertical transport within an aquatic canopy or benthic colony of varied height and density. Our results also suggested that the ascending secondary flow coupled to pressure-driven pore-water exfiltration may create rapid vertical advection between the sediment and water column, which could control the availability and distribution of nutrients and DIC within a canopy.

References

ACKERMAN, J. D. 1983. Current flow around *Zostera marina* plants and flowers: Implications for submarine pollination. Biol. Bull. **165:** 504.

———. 1986. Mechanistic implications for pollination in the marine angiosperm *Zostera marina.* Aquat. Bot. **24:** 343–353.

———. 1997. Submarine pollination in the marine angiosperm *Zostera marina* (Zosteraceae), II: Pollen transport in flow fields and capture by stigmas. Am. J. Bot. **84:** 1110–1119.

——— AND A. OKUBO. 1993. Reduced mixing in a marine macrophyte canopy. Funct. Ecol. **7:** 305–309.

BOEGER, R. T. 1992. The influence of substratum and water velocity on growth of *Ranunculus aquatilis* L. (Ranunculaceae). Aquat. Bot. **42:** 351–359.

BURKE, R., AND K. STOLZENBACH. 1983. Free surface flow through salt marsh grass. MIT-Sea Grant technical report, MITSG 83–16. Massachusetts Institute of Technology.

CAREY, D. A. 1983. Particle resuspension in the boundary layer induced by flow around polichaete tubes. Am. Zool. **11:** 137–145.

CHANCE, M. M., AND D. A. CRAIG. 1986. Hydrodynamics and behavior of Simuliidae larvae (Diptera). Can. J. Zool. **64:** 1295–1309.

ECKMAN, J. 1990. A model of passive settlement by planktonic

larvae onto bottoms of differing roughness. Limnol. Oceanogr. **35:** 887–901.

———, D. O. DUGGINS, AND A. T. SEWELL. 1989. Ecology of understory kelp environments, I: Effects of kelps on flow and particle transport near the bottom. J. Exp. Mar. Biol. Ecol. **129:** 173–187.

——— AND A. NOWELL. 1984. Boundary skin friction and sediment transport about an animal-tube mimic. Sedimentology **31:** 851–862.

ELLIOT, A., AND N. BROOKS. 1997*a*. Transfer of nonsorbing solutes to a streambed with bed forms: Theory. Water Resour. Res. **33:** 123–136.

——— AND ———. 1997*b*. Transfer of nonsorbing solutes to a streambed with bed forms: Laboratory experiment. Water Resour. Res. **33**(1):137–151.

FONSECA, M. S., AND J. A. CAHALAN. 1992. A preliminary evaluation of wave attenuation by four species of seagrass. Estuar. Coast. Shelf Sci. **35:** 565–576.

———, J. S. FISHER, J. C. ZIEMAN, AND G. W. THAYER. 1982. Influence of the seagrass *Zostera marina L.* on current flow. Estuar. Coast. Shelf Sci. **15:** 351–364.

FREEZE, R. A., AND J. A. CHERRY. 1979. Groundwater, p. 27. Prentice-Hall.

GAMBI, M. C., A. NOWELL, AND P. JUMARS. 1990. Flume observations on flow dynamics in *Zostera marina* (eelgrass) beds. Mar. Ecol. Progr. Ser. **61:** 159–169.

GRIZZLE, R. E., F. SHORT, C. NEWELL, H. HOVEN, AND L. KINDBLOM. 1996. Hydrodynamically induced synchronous waving of seagrasses: 'Monami' and its possible effects on larval mussel settlement. J. Exp. Mar. Biol. Ecol. **206:** 165–177.

GROVE, A., F. SHAIR, E. PETERSEN, AND A. ACRIVOS. 1964. An experimental investigation of the steady separated flow past a circular cylinder. J. Fluid Mech. **19:** 60–80.

GÜSS, S. 1998. Oxygen uptake at the sediment-water interface simultaneously measured using a flux chamber method and microelectrodes: Must a diffusive boundary layer exist? Estuar. Coast. Shelf Sci. **46:** 143–156.

HOSOKAWA, Y., AND T. HORIE. 1992. Flow and particulate nutrient removal by wetlands with emergent macrophyte, p. 1271–1282. *In* R. Vollenweider, R. Marchetti and R. Viviani [eds.], Marine coastal eutrophication: science of the total environment. Elsevier.

HUETTEL, M., AND G. GUST. 1992. Impact of bioroughness on interfacial solute exchange in permeable sediments. Mar. Ecol. Prog. Ser. **89:** 253–267.

———, W. ZIEBIS, AND S. FORSTER. 1996. Flow-induced uptake of particulate matter in permeable sediments. Limnol. Oceanogr. **41:** 309–322.

JOHNSON, A. S. 1988. Hydrodynamic study of the functional morphology of the benthic suspension feeder *Phoronopsis viridis* (Phoronida). Mar. Biol. **100:** 117–126.

———. 1990. Flow around phoronids: Consequences of a neighbor to suspension feeder. Limnol. Oceanogr. **35:** 1395–1401.

KNUTSON, P, R. BROCHU, W. SEELIG, AND M. INSKEEP. 1982. Wave damping in *Spartina alterniflora* marshes. Wetlands, **2:** 87–104.

KOCH, E. W. 1996. Hydrodynamics of a shallow *Thalassia testudinum* bed in Florida, USA, p. 105–109. *In* J. Kuo, R. Phillips, D. Walker, and H. Kirkman [eds.], Seagrass biology: Proceedings of an international workshop. Univ. Western Australia Press.

———. 1999. Preliminary evidence on the interdependent effect of currents and porewater geochemistry on *Thalassia testudinum* seedlings. Aquat. Bot. In press.

LEONARD, L., AND M. LUTHER. 1995. Flow hydrodynamics in tidal marsh canopies. Limnol. Oceanogr. **40:** 1474–1484.

LUO, S., T. GAN, AND Y. CHEW. 1996. Uniform flow past one (or two in tandem) finite length circular cylinder(s). J. Wind Eng. Indust. Aerodyn. **59:** 69–93.

MERRELL, K. C. 1996. The effect of flow and mixing on *Vallisneria* and its associated community in experimental mesocosms, p. 83. M.S. thesis, Univ. of Maryland.

MUNSON, B., D. YOUNG, AND T. OKIISHI. 1990. Fundamentals of fluid mechanics, p. 600-615. John Wiley & Sons.

NEPF, H. 1999. Drag, turbulence and diffusivity in flow through emergent vegetation. Water Resour. Res. In press.

———, C. MUGNIER, AND R. ZAVISTOSKI. 1997. The effects of vegetation on longitudinal dispersion. Estuar. Coast. Shelf Sci. **44:** 675–684.

NOWELL, A., AND M. CHURCH. 1979. Turbulent flow in a depth-limited boundary layer. J. Geophys. Res. **84:** 4816–4824.

PETRYK, S. 1969. Drag on cylinders in open channel flow. Ph.D. thesis, Colorado State Univ.

POWER, P. 1996. Effects of current velocity and substrate composition on growth of Texas wildrice (*Zizania texana*). Aquat. Bot. **55:** 199–204.

STARR, M. R. 1966. The characteristics of shear flows past a circular cylinder. Ph.D. thesis, Univ. of Bristol, U.K.

VOGEL, S. 1994. Life in moving fluids, 2nd ed., p. 217. Princeton Univ. Press.

WHITE, F. 1986. Fluid mechanics, 2nd ed, p. 331. McGraw-Hill.

WOO, H. G. C., J. E. CERMAK, AND J. A. PETERKA. 1989. Secondary flows and vortex formation around a circular cylinder in constant-shear flow. J. Fluid Mech. **204:** 523–542.

WORCESTER, S. E. 1995. Effects of eelgrass beds on advection and turbulent mixing in low current and low shoot density environments. Mar. Ecol. Progr. Ser. **126:** 223–232.

ZUKAUSKAS, A. 1987. Heat transfer from tubes in cross-flow. Adv. Heat Trans. **18:** 87–159.

Received: 30 July 1998
Accepted: 1 March 1999
Amended: 9 March 1999